ACS APPLIED MATERIALS & INTERFACES

www.acsami.org

Research Article

Transparent Supercapacitor Display with Redox-Active Metallo-Supramolecular Polymer Films

Sanjoy Mondal, Takefumi Yoshida, Subrata Maji, Katsuhiko Ariga, and Masayoshi Higuchi*

Cite This: *ACS Appl. Mater. Interfaces* 2020, 12, 16342−16349

Read Online

ACCESS | Metrics & More | Article Recommendations | Supporting Information

ABSTRACT: The use of metallo-supramolecular polymer (MSP) as a thin-film-based redox supercapacitor electrode material is reported for the first time. Fe(II)- and Ru(II)-based MSPs (polyFe and polyRu, respectively) were synthesized by complexation of appropriate metal salts with 4′,4″-(1,4-phenylene)bis-2,2′:6′,2″-terpyridine, and thin films of these polymers were prepared by spray coating onto an indium tin oxide glass substrate. A study of the energy storage performances of the polyFe and polyRu films in a nonaqueous electrolyte system revealed volumetric capacitances of ∼62.6 ± 3 F/cm^3 for polyFe and 98.5 ± 7 F/cm^3 for polyRu at a current density of 2 A/cm^3. To improve the energy storage performance over a wider potential range, asymmetric supercapacitor (ASC) displays were fabricated with suitable combinations of the MSPs as cathodic materials and Prussian blue as the anodic counter material in a sandwich configuration with a transparent polymeric ion gel as the electrolyte. The fabricated ASCs showed a maximum volumetric energy density (∼10−18 mW h/cm^3) that was higher than that of lithium thin-film batteries and a power density (7 W/cm^3) comparable to that of conventional electrolyte capacitors, with superb cyclic stability for 10 000 cycles. To demonstrate the practical use of the MSP, the illumination of a light-emitting diode bulb was powered by a laboratory-made device. This work should inspire the development of high-performance thin-film flexible supercapacitors based on MSPs as active cathodic materials.

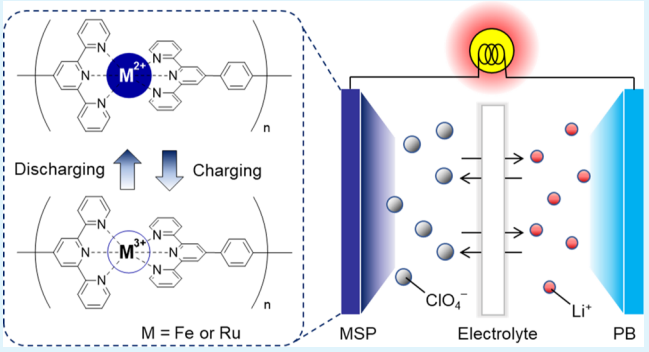

KEYWORDS: *metallo-supramolecular polymers, supercapacitors, transparent capacitors, thin-film, displays*

INTRODUCTION

The development of thin-film-based energy storage materials has received a great deal of attention because of the strong demand for their use as miniaturized portable energy storage devices of the next generation.[1−5] Unlike conventional capacitors or batteries, both high energy density and high power density are demanded of supercapacitors (SCs), in addition to rapid charge/discharge switching and long-term durability.[6−8] Many materials have been reported to be useful as electrode materials for conventional SCs, including carbonaceous materials,[5,9,10] metal oxides,[11,12] conducting polymers,[13−15] composites,[16,17] metal−covalent organic frameworks,[18,19] organic redox-active polymers[20−23] and so forth. However, there is still a demand for the development of high-performance thin-film energy storage materials for various microelectronics applications.[24,25] Although much effort has been devoted to the design of thin-film materials for high-performance energy storage applications, most of the resulting materials exhibit either good energy storage performance or film-forming properties, but not both. Materials that exhibit both good energy storage performance and are readily processable into films are rare. With this background, metallo-supramolecular polymers (MSPs) have attracted attention as superior alternatives for use as materials for transparent thin-film-based SC electrodes because of their excellent redox properties, controllable processability for thin-film formation, simple and high-yielding syntheses, and environmental and thermal stabilities.

The low energy density and poor cycle stability of SC devices is a serious problem in practical utilization. Compared with conventional SC devices, asymmetric SCs (ASCs) are capable of operating over a wider potential window, leading to substantial improvements in energy density and cycle stability.[26,27] Owing to their improved energy storage performance, the configuration of ASC devices is more demanding for hands-on applications. It is therefore important to choose optimal combinations of working and counter electrode materials in constructing redox ASC devices. Furthermore, to overcome the problem of a narrow potential window,

Received: December 22, 2019
Accepted: March 17, 2020
Published: March 17, 2020

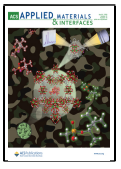

https://dx.doi.org/10.1021/acsami.9b23123
ACS Appl. Mater. Interfaces 2020, 12, 16342−16349

nonaqueous electrolytes are superior to aqueous electrolytes, as they can supply wider potential windows with appropriate electrode materials, leading to higher energy densities as well as enhanced cycle stabilities.[28,29] Moreover, the use of appropriate solid or semisolid nonaqueous electrolytes in devices is beneficial in terms of eliminating the problem of leakage of liquid electrolytes, increasing mechanical strength, enhancing flexibility, and reducing the total weight of devices, among other advantages.

MSPs consisting of metal ions and ditopic organic ligands are synthesized simply by complexation of the appropriate metal salt and ligand in solution.[30] We have reported that Fe- and Ru-based MSPs show reversible electrochromism through electrochemical redox reactions of the metal ions.[30,31] Furthermore, because of their high solubility and processability, these polymers can be readily formed into films by solution-based coating processes, such as simple spin coating or spray coating. When we investigated the performance of these electrochromic devices, we serendipitously discovered that the MSPs display a charge-storage function. In this study, we report for the first time the development of thin-film MSPs as electrode materials for redox SCs. Additionally, for practical utilization and improved energy storage performance, an asymmetric display has been fabricated consisting of a spray-printed MSP film as a cathodic material on the working electrode side and Prussian blue (PB) as an anodic material on the counter electrode side in a sandwich configuration with a nonaqueous ion-gel electrolyte.

EXPERIMENTAL SECTION

Materials. Iron(II) acetate [$Fe(OAc)_2$, >99.99%], *cis*-tetrakis-(dimethyl sulfoxide)dichlororuthenium(II) [$RuCl_2(DMSO)_4$; 96%], indium tin oxide (ITO)-coated glass substrates (resistivity 8−12 Ω/cm^2), anhydrous lithium perchlorate ($LiClO_4$), and PB were purchased from Sigma-Aldrich. 4′,4″-(1,4-Phenylene)bis-2,2′:6′,2″-terpyridine and poly(methyl methacrylate) [PMMA; average MW 350 kg/mol] were purchased from Tokyo Chemical Industry Co. Ltd. Propylene carbonate (PC), anhydrous acetic acid, spectroscopy-grade methanol (MeOH), and acetonitrile (ACN) were supplied by Wako Pure Chemical Industries, Ltd. (Osaka).

Synthesis of Polymers (PolyFe and PolyRu). We followed our previously reported procedure for the synthesis of polyFe and polyRu (Scheme 1).[31] An equimolar mixture of 4′,4″-(1,4-phenylene)bis-2,2′:6′,2″-terpyridine (200 mg, 0.37 mmol) and $Fe(OAc)_2$ (64 mg, 0.37 mmol) in acetic acid was refluxed overnight under a N_2-saturated atmosphere. The mixture was then cooled to room temperature and small amounts of insoluble residues were removed by filtration. The deep-blue filtrate of the polyFe solution in acetic acid was transferred to a Petri dish, and the acetic acid solvent was allowed to evaporate slowly at room temperature under atmospheric conditions. Finally, the product was dried under vacuum to obtain solid deep-blue polyFe in >93% yield.

Similarly, for the synthesis of polyRu, equimolar amounts of 4′,4″-(1,4-phenylene)bis-2,2′:6′,2″-terpyridine (200 mg, 0.37 mmol) and *cis*-$RuCl_2(DMSO)_4$ (179 mg, 0.37 mmol) were refluxed in ethylene glycol under a N_2-saturated atmosphere for 24 h. The mixture was cooled to room temperature, and the product was collected by precipitation with anhydrous tetrahydrofuran (THF) and then washed several times with THF. Finally, the solid product was dried in vacuum overnight to give pure polyRu in ∼90% yield.

Scheme 1. Preparation of polyFe and polyRu Polymers

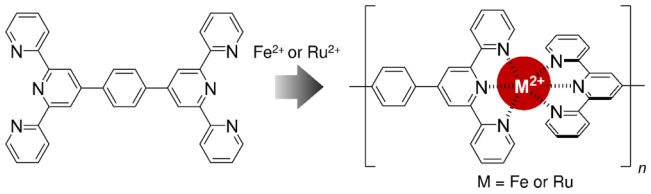

Preparation of MSP Films. Transparent ITO glass (resistivity 8−12 Ω/cm^2) was used as a conductive substrate. Before use, the ITO glass was cleaned by ultrasonication in acetone and then exposed to an ultraviolet (UV)−ozone chamber. A polymer-ink solution (3.5 mg/mL) was prepared by dissolving the appropriate solid polymer in methanol and filtered through a micropore syringe filter (polyvinylidene fluoride, 0.45 μm) to completely remove any small particles of insoluble residues. The resulting ink was then spray-coated onto the ITO glass substrate to produce a uniform thin bluish-violet (for polyFe) or red (for polyRu) film.

PB Film Preparation. The thin PB counter electrode layer was prepared by spin coating from a 10 mg/mL aqueous solution of PB onto an ITO glass substrate, previously cleaned by ultrasonication in acetone and exposed to a UV−ozone chamber for 30 min.

Device Fabrication. Each complete solid ASC device was fabricated with a sandwich configuration. Before the anode and cathode electrodes were combined, a semisolid ion-gel electrolyte was prepared by mixing PMMA, PC, $LiClO_4$, and ACN in a mass ratio of 20:7:3:70. This mixture was stirred continuously for 24 h at room temperature to give a clear colorless transparent viscous gel for use in device fabrication. A layer of the prepared viscous electrolyte ion gel was placed on the polymer-film-coated ITO glass and allowed to stand for 3−4 h. The gel electrolyte was then covered with PB-coated ITO glass to form a complete solid ASC device.

Calculations. On the basis of the galvanostatic charge/discharge (GCD) curve, the volumetric capacitance (C_v in F/cm^3), the energy density (E in W h/cm^3), and the power density (P in W/cm^3) of the polymer films were calculated using eqs 1−3, respectively[2,3,32,33]

$$C_v = \frac{i}{v} \times \frac{\Delta t}{\Delta V} \quad (1)$$

$$E = \frac{1}{2} \times C_v \times \frac{(\Delta V^2)}{3600} \quad (2)$$

$$P = \frac{E}{\Delta t} \times 3600 \quad (3)$$

Here, i is the current (A), Δt is the discharge time (s), ΔV is the voltage window (V), and v is the volume of the polymer film (cm^3).

RESULTS AND DISCUSSION

Fe- and Ru-based MSPs (polyFe and polyRu) were synthesized as described in our previous report.[31] Their optical properties were characterized by ultraviolet−visible (UV−vis) spectroscopy (Figure 1). Strong absorption bands appeared at 502 nm for polyRu and 586 nm for polyFe. These absorptions

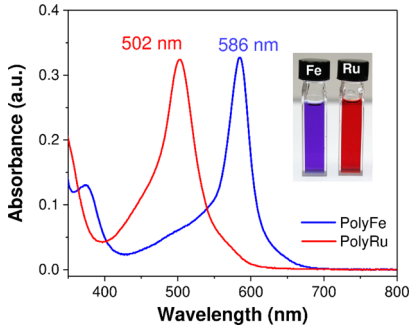

Figure 1. UV−vis spectra of methanolic solutions of the polymers (inset image: the blue and red colors of the solutions of polyFe and polyRu, respectively).

https://dx.doi.org/10.1021/acsami.9b23123
ACS Appl. Mater. Interfaces 2020, 12, 16342−16349

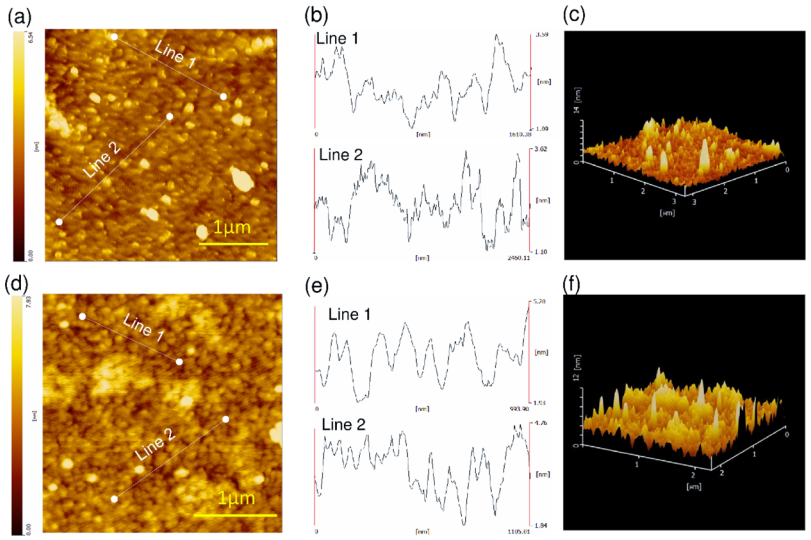

Figure 2. AFM topographic images (a,d), the corresponding cross-sectional analysis views (b,e), and 3D views (c,f) of spray-coated polyFe (top) and polyRu (bottom) films on a mica surface.

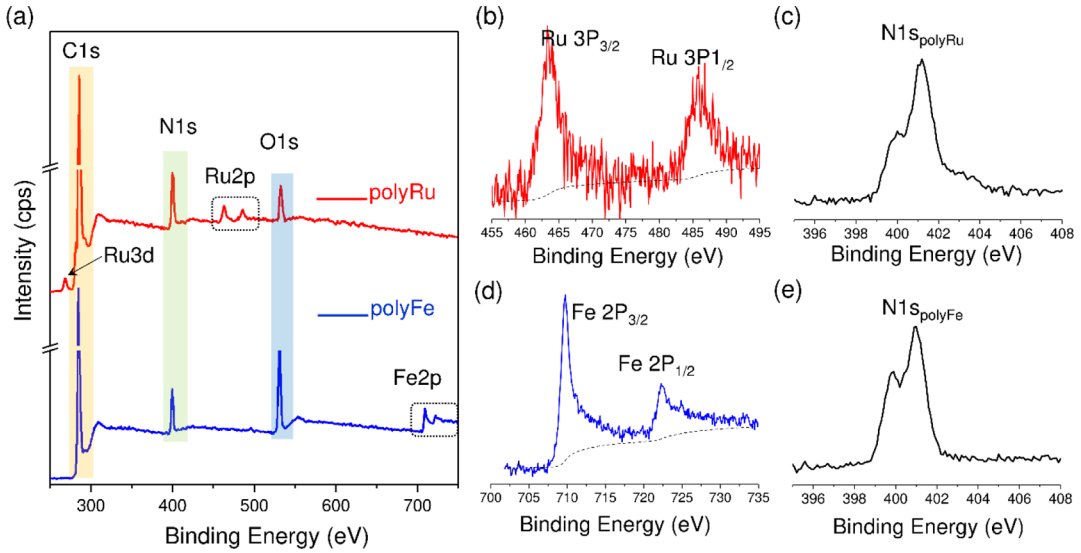

Figure 3. (a) Wide-scale XPS of polyFe and polyRu; narrow-scale XPS focusing on (b) Ru 3p, (c) N $1s_{polyRu,}$ (d) Fe 2p, and (e) N $1s_{polyFe}$.

are caused by the characteristic metal-to-ligand charge transfer of the bisterpyridine−metal (Fe^{2+}, Ru^{2+}) complexes, which exhibit a quasi-octahedral geometry.[31,34] A significant color change induced by the two different metal ions resulted in the development of brilliant blue and red colors for polyFe and polyRu, respectively (see inset image of Figure 1).

The morphology and surface topology of the polyFe and polyRu films were investigated by atomic force microscopy (AFM), as shown in Figure 2. Polymer films produced by spray coating onto a mica surface showed a nanometer-size (approximately 10−15 nm) assembly with a spherical dot-like morphology (Figures 2a,d). Cross-sectional analyses of the assemblies (Figure 2b,e) confirmed that the surfaces were rough. Three-dimensional (3D) views of the topographic images (Figure 2c,f) further revealed that the polymers had roughly flat surfaces.

The presence of the elements and their composition in the polymers were examined by X-ray photoelectron spectroscopy (XPS), as shown in Figure 3. The peaks at 286, 400, and 532 eV, which are characteristic peaks for C 1s, N 1s, and O 1s, respectively, were perfectly matched in the wide-scale spectra of the two polymers.[17] The peaks at ∼709 and 722 eV for polyFe are characteristic peaks for Fe $2p_{3/2}$ and Fe $2p_{1/2}$, respectively, indicating the presence of Fe in the polymer (Figure 3a,d).[35] Similarly, the peaks at ∼280, 463, and 486 eV for polyRu are characteristic peaks for Ru 3d, Ru $3p_{3/2}$, and Ru $3p_{1/2}$, respectively, demonstrating the presence of Ru in this polymer (Figures 3a,b).[36] Importantly, the nitrogen-to-metal (N/Fe or N/Ru) atomic ratios calculated by considering the peak areas were found to be 5.9:1 (N/Fe) for polyFe and 5.6:1 (N/Ru) for polyRu, compared with the ideal values of N/Fe = 6:1 and N/Ru = 6:1, respectively.

The morphology and elemental composition (especially the N-to-metal atomic percentage ratio) of the polymers were further analyzed by scanning electron microscopy (SEM), transmission electron microscopy (TEM), and a corresponding energy dispersive spectroscopy (EDS) study (see Figure S1 in the Supporting Information). The EDS analyses confirmed the elemental compositions of the polymers qualitatively and quantitatively. In the two polymers, the N-to-metal (Fe or Ru)

https://dx.doi.org/10.1021/acsami.9b23123
ACS Appl. Mater. Interfaces 2020, 12, 16342−16349

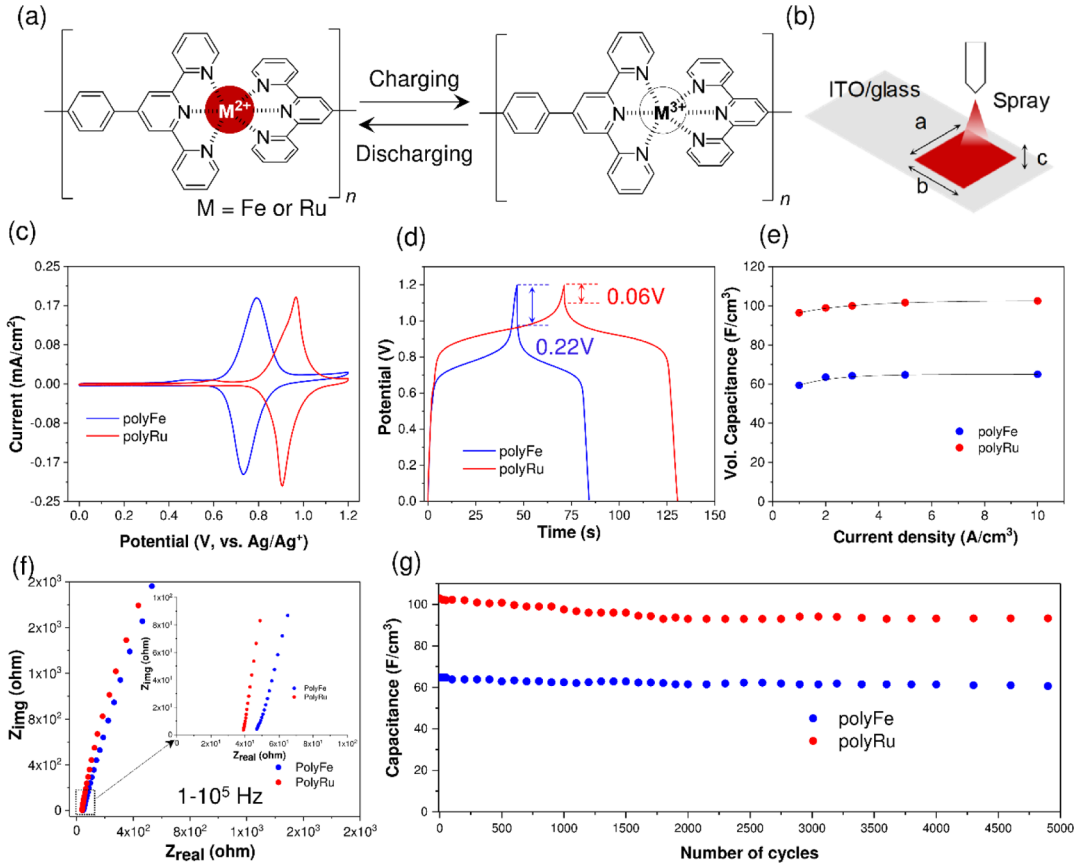

Figure 4. (a) Structural changes in the polymers during charge/discharge. (b) Schematic illustration of the preparation of the polymer film. (c–g) Three-electrode electrochemical study of polyFe (blue line) and polyRu (red line): (c) CV study at a scan speed of 20 mV/s; (d) GCD profile at a current density of 2 A/cm^3; (e) volumetric capacitance versus current density plot; (f) EIS study (Nyquist plot) in the range 0.1 to 10^5 Hz; (g) GCD cyclic performance over 5000 cycles at 10 A/cm^3.

atomic percentage ratios were 6.2:1 for polyFe and 5.7:1 for polyRu, strongly suggesting that the metal was bound to the ligand in a hexacoordinate fashion. Thermogravimetric analysis (TGA) showed that polyFe and polyRu were stable from room temperature to ~550 °C under a N_2-saturated atmosphere (see Supporting Information, Figure S2). An initial small weight loss at about 80–100 °C corresponded to the evaporation of trace amounts of adsorbed moisture or solvent from the surfaces of the polymers. On increasing the temperature beyond 100 °C, slow degradation occurred for both polymers, and a sharp weight loss was observed at about 370–420 °C for polyFe, with 48% weight retention. It is noteworthy that polyFe showed a 52% weight loss (i.e., 48% retention) and polyRu showed a 36% weight loss (i.e., 64% retention) above 550 °C. Powder X-ray diffraction (XRD) analyses confirmed that both polymers had low degrees of crystallinity (Figure S3, Supporting Information).

Electrochemical Properties and Energy Storage Performance of the Polymers. The electrochemical properties of the polymer films were examined by using a classical three-electrode system and a two-electrode technique in a nonaqueous electrolyte system.[17,37−40] The volumetric energy storage performance of polymer films was tested by cyclic voltammetry (CV), GCD studies, and electrochemical impedance spectroscopy (EIS) analysis. During electrochemical charge/discharge of the polymers, simple oxidation/reduction of the metal center (Fe^{2+} or Ru^{2+}) occurs, as shown schematically in Figure 4a. The oxidation and reduction peak current densities were proportional to the square root of the scan rate, implying a diffusion-controlled rate capability redox mechanism at the electrolyte–polymer interface (Figure S4, Supporting Information). The volume ($a \times b \times c$) of the polymer films was measured by considering their area and thickness, as shown in Figure 4b; the thickness of the films was determined by means of an absorption-versus-thickness study (Figure S5 for polyFe and Figure S6 for polyRu; see Supporting Information).

CV is a useful electrochemical research method that is widely used to investigate the electrochemical behavior, mechanism, and kinetics of electrode materials. A three-electrode technique was used to evaluate the electrochemical properties of polyFe and polyRu in the 0–1.2 V potential window at a scan rate of 20 mV/s in 0.1 M $LiClO_4$ ACN electrolyte solution (Figure 4c). The CV study of the polymers clearly showed the presence of excellent reversible redox behavior in the 0.71–0.81 V ($E_{1/2}$ = 0.755 V vs Ag/Ag^+) region for polyFe and in the 0.88–0.98 V ($E_{1/2}$ = 0.93 V vs Ag/Ag^+) region for polyRu. The strong oxidation peak at 0.81 V was attributed to a Fe^{2+}-to-Fe^{3+} transition of polyFe, and the reduction peak at 0.71 V was attributed to a Fe^{3+}-to-Fe^{2+} conversion. Similarly, for polyRu, the strong oxidation peak at 0.88 V was attributed to the Ru^{2+}-to-Ru^{3+} conversion, and the reduction peak at 0.98 V was attributed to the Ru^{3+}-to-Ru^{2+} transition. The typical reversible redox signals in the CV study indicated that the polymers showed a pseudocapacitive charge-storage performance.

https://dx.doi.org/10.1021/acsami.9b23123
ACS Appl. Mater. Interfaces 2020, 12, 16342−16349

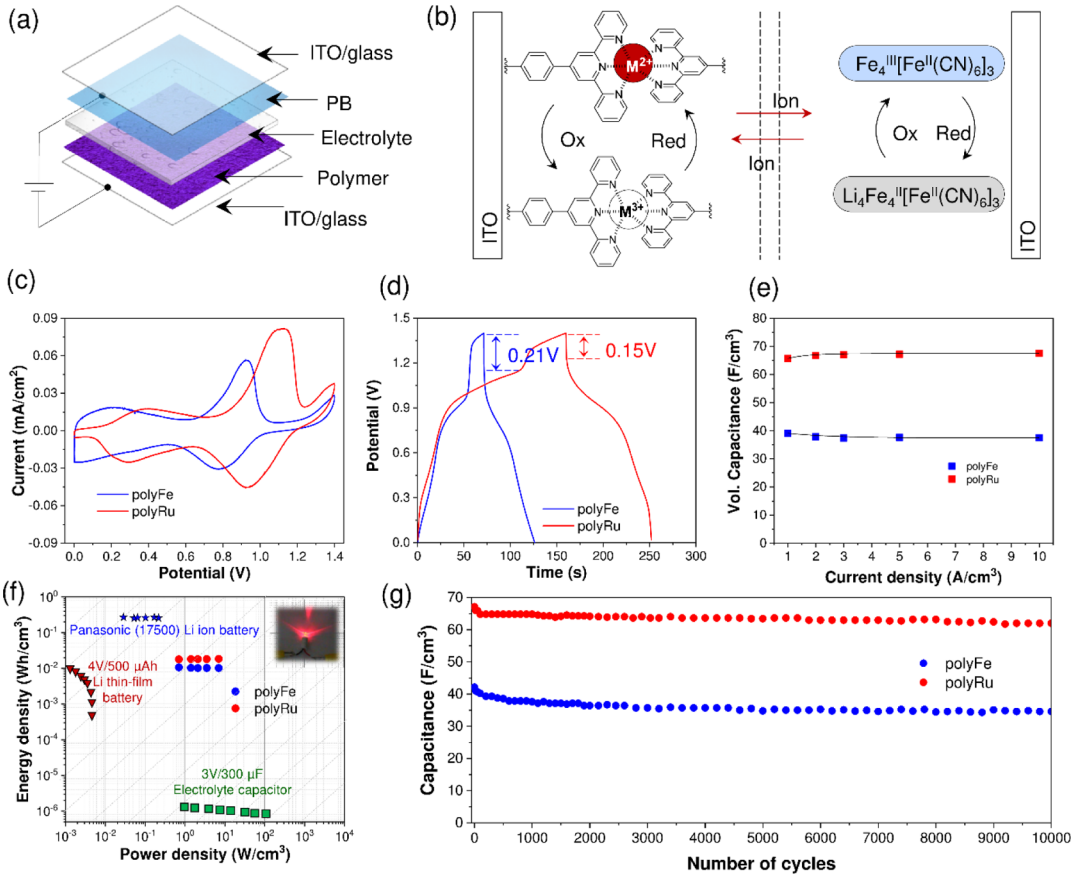

Figure 5. (a) Schematic representation of the structure of the ASC device. (b) Electrochemical redox reaction between the two electrodes. (c) CV study at 20 mV/s. (d) GCD study at a current density of 1 A/cm^3. (e) Volumetric capacitance vs current density. (f) Ragone plot. (g) Stability over 10,000 charge/discharge cycles.

The charge-storage ability and mechanism of the polymers films were examined by the GCD method at a current density of 2 A/cm^3 within the 0−1.2 V potential window, as shown in Figure 4d. Here, the polymer film-coated ITO glass served as the working electrode, freshly prepared Ag/Ag$^+$ served as the reference electrode, and a Pt wire acted as the counter electrode. The active area of both films was 1 × 1 cm^2, with thicknesses of ∼168 ± 12 nm for polyFe and ∼110 ± 10 nm for polyRu. The nonlinear charge/discharge curve clearly confirmed the presence of a battery-like charge-storage mechanism for the electrode films, which is dominated by a faradic redox reaction on the surface of the polymers.[17,41] The volumetric capacitances calculated from the GCD curve by using eq 1 were 62.6 ± 3 F/cm^3 for polyFe and 98.5 ± 7 F/cm^3 for polyRu at a current density of 2 A/cm^3. Both polymer films showed little *IR* drop: 0.22 V for the polyFe film and 0.06 V for the polyRu film in the 0−1.2 V potential window. As we discussed earlier, our polymers showed a predominant battery-like energy storage behavior through a faradic redox reaction with $E_{1/2}$ = 0.755 V for polyFe and $E_{1/2}$ = 0.93 V for polyRu. The polymers showed a negligible *IR* drop in their GCD behavior in the redox region only. On extending the potential window from the redox region, the *IR* drop gradually increased (Figure S7, see Supporting Information). For the purpose of comparison, we used the same potential windows (0−1.2 V) for both polymers. The *IR* drops in various potential windows for both polymers are summarized in Table S1 (see Supporting Information). The results of the GCD tests at various current densities (2−10 A/cm^3), as shown in Figure S8 (Supporting Information), implied that a nonlinear faradic transformation occurs over this range of current densities for both polymers. The energy storage performances of the polymer films are summarized in Table S2 (Supporting Information). Remarkably, on increasing the current density, the capacitance value remained unchanged, indicating that the polymers have a rapid charge-storage ability (Figure 4e). Furthermore, the unchanged specific capacitance over current density also implies a high rate of charge-storage performance for both polymers (Figure S10, see Supporting Information). Additionally, we measured the areal capacitances for polyFe and polyRu films (active area: 1.0 × 1.0 cm^2) as 1.51 and 2.02 mF/cm^2, respectively, at a current density of 0.1 mA/cm^2 with a Coulombic efficiency of <90% (Figure S9, Supporting Information). The areal capacitance and Coulombic efficiency for both polymers are summarized in Table S3 (Supporting Information).

To examine the charge-transport process that occurs on the surfaces of the polymers, we carried out an EIS study in the frequency range 1 to 10^5 Hz (Figure 4f). The high-frequency region generally corresponds to charge-transfer processes, whereas the low-frequency region is dominated by mass-transfer processes.[17,42] A negligible semicircular behavior was observed in the high-frequency region of the Nyquist plot, indicating a low interfacial charge-transfer resistance (R_{CT}). The values of R_{CT} for polyFe and polyRu were 4.17 and 3.45 Ω, respectively. In the high-frequency region, the equivalent series resistances (R_e) of polyFe and polyRu were 46.9 and 39 Ω, respectively. The slope (about 70−80°) of the Nyquist plot in the low-frequency region indicated an ideal capacitive

https://dx.doi.org/10.1021/acsami.9b23123
ACS Appl. Mater. Interfaces 2020, 12, 16342−16349

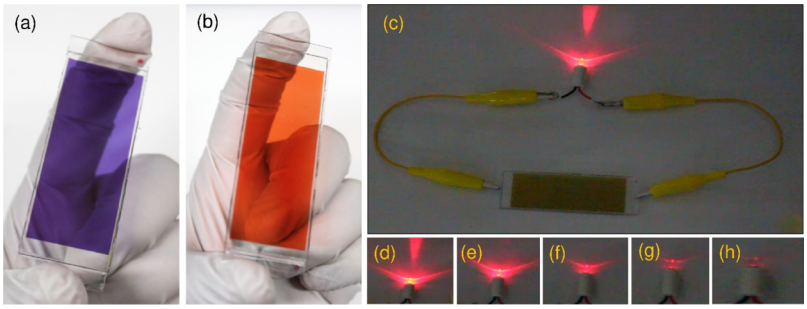

Figure 6. (a,b) Photographs of laboratory-made polyFe- and polyRu-based AHDs, respectively. (c) Optical image of an LED powered by the RuAHD at various times: (d) 0.5, (e) 1, (f) 2, (g) 3, and (h) 5 min.

behavior of the polymers.[43,44] The cyclic performance of the polymer films was tested over 5000 cycles at a current density of 10 A/cm^3 in the solution state. Figure 4g shows an almost negligible loss of properties (~6% for polyFe and ~8% for polyRu), implying that these materials have good electrochemical stability.

Energy Storage Performance in the Asymmetric Hybrid Devices. To improve the energy storage performance and long-term cycle stability, it was necessary to fabricate an ASC device.[26,27,43−48] Note that a perfect combination of electrode materials is important in producing a redox ASC. We constructed ASC devices with our synthesized MSPs as cathodic materials on the working electrode side and PB as the anodic material on the counter electrode side as a suitable combination in a sandwich configuration with a polymeric nonaqueous ion gel as the electrolyte (Figure 5a). The classical two-electrode technique was used to measure the charge-storage capabilities of the polyFe- and polyRu-based asymmetric devices. The electrochemical behavior of PB was characterized separately by CV analysis under identical conditions (Figure S11, Supporting Information). The electrochemical behavior of the MSPs without PB in the device state is summarized in Figure S12 (Supporting Information). The electrochemical redox reaction between the cathode and the anode during charge/discharge switching is illustrated schematically in Figure 5b. In the asymmetric hybrid device, simultaneous but opposite redox reactions occur between the two electrodes.

The electrochemical behavior and charge-storage ability of polyFe and polyRu in the asymmetric hybrid devices were measured by CV and GCD experiments. In the CV analysis, it was observed that both devices showed charge/discharge behavior through redox reactions in the 0−1.4 V potential window (Figure 5c). The polyFe-based asymmetric hybrid device (FeAHD) showed charging by oxidation at ~0.92 V and discharge by reduction at ~0.77 V. Similarly, the polyRu-based asymmetric hybrid device (RuAHD) charged at ~1.2 V and discharged at ~0.92 V through a redox reaction. The charge/discharge behavior of both devices was further characterized by a GCD study at a current density of 1 A/cm^3 in the same potential range (0−1.4 V), the results of which are shown in Figure 5d. The nonlinear shape of the GCD curve indicates the existence of dominant battery-like properties for both devices. By using eq 1 and the GCD curve, we calculated the volumetric capacitances of FeAHD and RuAHD to be 39 ± 2 and 65 ± 5 F/cm^3, respectively. On increasing the current density, the volumetric capacitance remained unchanged for both devices, implying a rapid charge/discharge ability (Figure 5e). The GCD curves at various current densities for the two devices are shown in Figure S13 (see Supporting Information). The Ragone plot is the best method for evaluating the energy storage performance of devices for practical applications.[1−3,24] The energy density and the power density of our fabricated asymmetric hybrid devices are shown in the Ragone plots in Figure 5f. The volumetric energy density and power density for the two devices were calculated by using eqs 2 and 3, respectively. The maximum volumetric energy density reached 10.6 mW/cm^3 for the polyFe-based AHD and 17.8 mW/cm^3 for the polyRu-based AHD at a power density of 0.7 W h/cm^3. A comparison study with a previously reported work is summarized in Table S4 (Supporting Information). Remarkably, our MSP thin-film-based devices delivered an overall better energy storage performance than a lithium thin-film battery,[5] an electrolytic capacitor,[2,3] an activated-carbon electrical double-layer capacitor,[49] Panasonic Li-ion batteries,[50] and other types of thin-film-based energy storage devices. The long-term cyclic performance of the MSP-based hybrid devices showed good electrochemical stability, with ~85% (FeAHD) and ~92% (RuAHD) retention of the initial volumetric capacitance after 10 000 GCD cycles at a current density of 10 A/cm^3 (Figure 5g). The unchanged morphology and elemental composition (especially N-to-metal) of both polymers before and after 10,000 GCD cycles also suggest a strong cyclic stability (Figure S14, Supporting Information).

Next, we fabricated the polyFe- and polyRu-based laboratory-made asymmetric devices shown in Figure 6a,b, respectively, with dimensions of ~2.5 × 1.5 cm^2. As a real application, we demonstrated that a light-emitting diode (LED) bulb could be lit by the polyRu-based device (Figure 6c). After the device had been fully charged, the LED glowed brightly for 30 s, and then its intensity fell slowly for up to 5 min (Figure 6d−h).

CONCLUSIONS

In summary, we have developed, for the first time, high-performance SCs with Fe(II)- or Ru(II)-based MSPs as thin redox electrode materials. We succeeded in preparing uniform, binder-free, thin films of polymer inks by a spray-coating technique, and we fabricated devices with a nonaqueous electrolyte. The charge-storage ability, mechanism, and lifetime of the spray-printed polymer films were evaluated by CV, GCD, and EIS studies in the solution state. The redox-active MSP films showed a high charge-storage capability through a redox mechanism with a maximum volumetric capacitance of 62.5 ± 5.4 F/cm^3 for polyFe and 98.5 ± 8 F/cm^3 for polyRu, with a >92% lifecycle stability over 5000 cycles in the solution state. Asymmetric devices were fabricated with a suitable combination of a synthesized MSP as a cathodic electrode

https://dx.doi.org/10.1021/acsami.9b23123
ACS Appl. Mater. Interfaces 2020, 12, 16342−16349

material, PB as an anodic electrode material, and a central nonaqueous electrolyte in a sandwich configuration. These MSP-based asymmetric devices exhibited a maximum energy density of 10−18 mW h/cm^3 and a maximum power density of 7 W/cm^3 with superb electrochemical stability for more than 10,000 cycles (85−92% retention of the initial volumetric capacitance). Finally, we demonstrate that an LED bulb could be illuminated for ∼5 min by a laboratory-made device of dimensions ∼2.5 × 1.5 cm^2 when this was fully charged. We believe that this study not only demonstrated that new MSPs can act as a novel type of thin-film SC electrode material but also demonstrated the potential volumetric energy storage performance of spray-printed industrial thin-film-based micro-SC devices of the near future.

■ ASSOCIATED CONTENT

Supporting Information

The Supporting Information is available free of charge at https://pubs.acs.org/doi/10.1021/acsami.9b23123.

TEM, SEM, TGA, XRD, film thickness, areal capacitance, Coulombic efficiency, scan-dependent CV data, results of GCD studies at various current densities, electrochemical properties of PB, and a table showing comparisons with previous results (PDF)

■ AUTHOR INFORMATION

Corresponding Author

Masayoshi Higuchi − *Electronic Functional Macromolecules Group, National Institute for Materials Science (NIMS), Tsukuba 305-0044, Japan;* orcid.org/0000-0001-9877-1134; Email: HIGUCHI.Masayoshi@nims.go.jp

Authors

Sanjoy Mondal − *Electronic Functional Macromolecules Group, National Institute for Materials Science (NIMS), Tsukuba 305-0044, Japan;* orcid.org/0000-0002-4391-6356

Takefumi Yoshida − *Electronic Functional Macromolecules Group, National Institute for Materials Science (NIMS), Tsukuba 305-0044, Japan;* orcid.org/0000-0003-3479-7890

Subrata Maji − *World Premier International Research Center for Materials Nanoarchitectonics (WPI-MANA), National Institute for Materials Science (NIMS), Tsukuba 305-0044, Japan*

Katsuhiko Ariga − *World Premier International Research Center for Materials Nanoarchitectonics (WPI-MANA), National Institute for Materials Science (NIMS), Tsukuba 305-0044, Japan; Department of Advanced Materials Science, Graduate School of Frontier Sciences, The University of Tokyo, Kashiwa, Chiba 277-8561, Japan;* orcid.org/0000-0002-2445-2955

Complete contact information is available at: https://pubs.acs.org/10.1021/acsami.9b23123

Notes

The authors declare no competing financial interest.

■ ACKNOWLEDGMENTS

This research was financially supported by the CREST project (grant number: JPMJCR1533) from the Japan Science and Technology Agency. The XPS study was conducted at the AIST Nano-Processing Facility, supported by the 'Nanotechnology Platform Program' of the Ministry of Education, Culture, Sports, Science and Technology (MEXT), Japan.

■ REFERENCES

(1) Simon, P.; Gogotsi, Y. Materials for Electrochemical Capacitors. *Nat. Mater.* **2008**, *7*, 845.

(2) El-Kady, M. F.; Strong, V.; Dubin, S.; Kaner, R. B. Laser Scribing of High-Performance and Flexible Graphene-Based Electrochemical Capacitors. *Science* **2012**, *335*, 1326.

(3) Wu, Z.-S.; Parvez, K.; Feng, X.; Müllen, K. Graphene-Based In-Plane Micro-Supercapacitors with High Power and Energy Densities. *Nat. Commun.* **2013**, *4*, 2487.

(4) Qi, D.; Liu, Y.; Liu, Z.; Zhang, L.; Chen, X. Design of Architectures and Materials in In-Plane Micro-Supercapacitors: Current Status and Future Challenges. *Adv. Mater.* **2017**, *29*, 1602802.

(5) Kaempgen, M.; Chan, C. K.; Ma, J.; Cui, Y.; Gruner, G. Printable Thin Film Supercapacitors Using Single-Walled Carbon Nanotubes. *Nano Lett.* **2009**, *9*, 1872.

(6) Simon, P.; Gogotsi, Y.; Dunn, B. Where Do Batteries End and Supercapacitors Begin? *Science* **2014**, *343*, 1210.

(7) Zhang, L. L.; Zhao, X. S. Carbon-Based Materials as Supercapacitor Electrodes. *Chem. Soc. Rev.* **2009**, *38*, 2520.

(8) Gogotsi, Y.; Simon, P. Materials Science. True Performance Metrics in Electrochemical Energy Storage. *Science* **2011**, *334*, 917.

(9) Huang, P.; Lethien, C.; Pinaud, S.; Brousse, K.; Laloo, R.; Turq, V.; Respaud, M.; Demortiere, A.; Daffos, B.; Taberna, P. L.; Chaudret, B.; Gogotsi, Y.; Simon, P. On-Chip and Freestanding Elastic Carbon Films for Micro-Supercapacitors. *Science* **2016**, *351*, 691.

(10) Zhang, L. L.; Zhou, R.; Zhao, X. S. Graphene-Based Materials as Supercapacitor Electrodes. *J. Mater. Chem.* **2010**, *20*, 5983.

(11) Lee, J. W.; Hall, A. S.; Kim, J.-D.; Mallouk, T. E. A Facile and Template-Free Hydrothermal Synthesis of Mn_3O_4 Nanorods on Graphene Sheets for Supercapacitor Electrodes with Long Cycle Stability. *Chem. Mater.* **2012**, *24*, 1158.

(12) Ho, K.-C.; Lin, L.-Y. A review of electrode materials based on core-shell nanostructures for electrochemical supercapacitors. *J. Mater. Chem. A* **2019**, *7*, 3516.

(13) Baker, C. O.; Huang, X.; Nelson, W.; Kaner, R. B. Polyaniline Nanofibers: Broadening Applications for Conducting Polymers. *Chem. Soc. Rev.* **2017**, *46*, 1510.

(14) Bryan, A. M.; Santino, L. M.; Lu, Y.; Acharya, S.; D'Arcy, J. M. Conducting Polymers for Pseudocapacitive Energy Storage. *Chem. Mater.* **2016**, *28*, 5989.

(15) Österholm, A. M.; Shen, D. E.; Dyer, A. L.; Reynolds, J. R. Optimization of PEDOT Films in Ionic Liquid Supercapacitors: Demonstration as a Power Source for Polymer Electrochromic Devices. *ACS Appl. Mater. Interfaces* **2013**, *5*, 13432.

(16) Mondal, S.; Rana, U.; Malik, S. Graphene Quantum Dot-Doped Polyaniline Nanofiber as High Performance Supercapacitor Electrode Materials. *Chem. Commun.* **2015**, *51*, 12365.

(17) Mondal, S.; Rana, U.; Malik, S. Reduced Graphene Oxide/Fe_3O_4/Polyaniline Nanostructures as Electrode Materials for an All-Solid-State Hybrid Supercapacitor. *J. Phys. Chem. C* **2017**, *121*, 7573.

(18) Halder, A.; Ghosh, M.; Abdul, K. M.; Bera, S.; Addicoat, M.; Sasmal, H. S.; Karak, S.; Kurungot, S.; Banerjee, R. Interlayer Hydrogen-Bonded Covalent Organic Frameworks as High-Performance Supercapacitors. *J. Am. Chem. Soc.* **2018**, *140*, 10941.

(19) Wang, R.; Jin, D.; Zhang, Y.; Wang, S.; Lang, J.; Yan, X.; Zhang, L. Engineering Metal Organic Framework Derived 3D Nanostructures for High Performance Hybrid Supercapacitors. *J. Mater. Chem. A* **2017**, *5*, 292.

(20) Muench, S.; Wild, A.; Friebe, C.; Häupler, B.; Janoschka, T.; Schubert, U. S. Polymer-Based Organic Batteries. *Chem. Rev.* **2016**, *116*, 9438.

(21) Winsberg, J.; Hagemann, T.; Janoschka, T.; Hager, M. D.; Schubert, U. S. Redox-Flow Batteries: From Metals to Organic Redox-Active Materials. *Angew. Chem., Int. Ed.* **2017**, *56*, 686.

(22) Schmidt, D.; Hager, M. D.; Schubert, U. S. Photo-Rechargeable Electric Energy Storage Systems. *Adv. Energy Mater.* **2016**, *6*, 1500369.

(23) Winsberg, J.; Janoschka, T.; Morgenstern, S.; Hagemann, T.; Muench, S.; Hauffman, G.; Gohy, J.-F.; Hager, M. D.; Schubert, U. S. Poly(TEMPO)/Zinc Hybrid-Flow Battery: A Novel, "Green," High Voltage, and Safe Energy Storage System. *Adv. Mater.* **2016**, *28*, 2238.
(24) Li, J.; Delekta, S. S.; Zhang, P.; Yang, S.; Lohe, M. R.; Zhuang, X.; Feng, X.; Östling, M. Scalable Fabrication and Integration of Graphene Microsupercapacitors through Full Inkjet Printing. *ACS Nano* **2017**, *11*, 8249.
(25) Lv, Q.; Chi, K.; Zhang, Y.; Xiao, F.; Xiao, J.; Wang, S.; Loh, K. P. Ultrafast Charge/Discharge Solid-State Thin-Film Supercapacitors via Regulating the Microstructure of Transition-Metal-Oxide. *J. Mater. Chem. A* **2017**, *5*, 2759.
(26) Feng, J.-X.; Ye, S.-H.; Wang, A.-L.; Lu, X.-F.; Tong, Y.-X.; Li, G.-R. Flexible Cellulose Paper-Based Asymmetrical Thin Film Supercapacitors with High-Performance for Electrochemical Energy Storage. *Adv. Funct. Mater.* **2014**, *24*, 7093. Corrigendum. *Adv. Funct. Mater.* **2019**, *29*, 1905171 DOI: 10.1002/adfm.201905171
(27) Shao, Y.; El-Kady, M. F.; Sun, J.; Li, Y.; Zhang, Q.; Zhu, M.; Wang, H.; Dunn, B.; Kaner, R. B. Design and Mechanisms of Asymmetric Supercapacitors. *Chem. Rev.* **2018**, *118*, 9233.
(28) Li, Y.; Lu, J. Metal-Air Batteries: Will They Be the Future Electrochemical Energy Storage Device of Choice? *ACS Energy Lett.* **2017**, *2*, 1370.
(29) Han, S.-D.; Rajput, N. N.; Qu, X.; Pan, B.; He, M.; Ferrandon, M. S.; Liao, C.; Persson, K. A.; Burrell, A. K. Origin of Electrochemical, Structural, and Transport Properties in Nonaqueous Zinc Electrolytes. *ACS Appl. Mater. Interfaces* **2016**, *8*, 3021.
(30) Higuchi, M. Stimuli-Responsive Metallo-Supramolecular Polymer Films: Design, Synthesis and Device Fabrication. *J. Mater. Chem. C* **2014**, *2*, 9331.
(31) Han, F. S.; Higuchi, M.; Kurth, D. G. Metallosupramolecular Polyelectrolytes Self-Assembled from Various Pyridine Ring-Substituted Bisterpyridines and Metal Ions: Photophysical, Electrochemical, and Electrochromic Properties. *J. Am. Chem. Soc.* **2008**, *130*, 2073.
(32) Feng, D.; Lei, T.; Lukatskaya, M. R.; Park, J.; Huang, Z.; Lee, M.; Shaw, L.; Chen, S.; Yakovenko, A. A.; Kulkarni, A.; Xiao, J.; Fredrickson, K.; Tok, J. B.; Zou, X.; Cui, Y.; Bao, Z. Robust and Conductive Two-Dimensional Metal-Organic Frameworks with Exceptionally High Volumetric and Areal Capacitance. *Nat. Energy* **2018**, *3*, 30.
(33) Zhang, P.; Li, Y.; Wang, G.; Wang, F.; Yang, S.; Zhu, F.; Zhuang, X.; Schmidt, O. G.; Feng, X. Zn-Ion Hybrid Micro-Supercapacitors with Ultrahigh Areal Energy Density and Long-Term Durability. *Adv. Mater.* **2019**, *31*, 1806005.
(34) Sénéchal-David, K.; Leonard, J. P.; Plush, S. E.; Gunnlaugsson, T. Supramolecular Self-Assembly of Mixed f−d Metal Ion Conjugates. *Org. Lett.* **2006**, *8*, 2727.
(35) Takada, K.; Sakamoto, R.; Yi, S.-T.; Katagiri, S.; Kambe, T.; Nishihara, H. Electrochromic Bis(terpyridine)metal Complex Nanosheets. *J. Am. Chem. Soc.* **2015**, *137*, 4681.
(36) Hou, C.-C.; Li, T.-T.; Cao, S.; Chen, Y.; Fu, W.-F. Incorporation of a $[Ru(dcbpy)(bpy)_2]^{2+}$ Photosensitizer and a $Pt(dcbpy)Cl_2$ Catalyst into Metal−Organic Frameworks for Photocatalytic Hydrogen Evolution from Aqueous Solution. *J. Mater. Chem. A* **2015**, *3*, 10386.
(37) Anothumakkool, B.; Torris, A. T. A.; Bhange, S. N.; Unni, S. M.; Badiger, M. V.; Kurungot, S. Design of a High Performance Thin All-Solid-State Supercapacitor Mimicking the Active Interface of Its Liquid-State Counterpart. *ACS Appl. Mater. Interfaces* **2013**, *5*, 13397.
(38) Wang, A.-L.; Xu, H.; Feng, J.-X.; Ding, L.-X.; Tong, Y.-X.; Li, G.-R. Design of Pd/PANI/Pd Sandwich-Structured Nanotube Array Catalysts with Special Shape Effects and Synergistic Effects for Ethanol Electrooxidation. *J. Am. Chem. Soc.* **2013**, *135*, 10703.
(39) Feng, J.-X.; Tong, S.-Y.; Tong, Y.-X.; Li, G.-R. Pt-like Hydrogen Evolution Electrocatalysis on PANI/CoP Hybrid Nanowires by Weakening the Shackles of Hydrogen Ions on the Surfaces of Catalysts. *J. Am. Chem. Soc.* **2018**, *140*, 5118.
(40) Feng, J.-X.; Xu, H.; Ye, S.-H.; Ouyang, G.; Tong, Y.-X.; Li, G.-R. Silica-Polypyrrole Hybrids as High-Performance Metal-Free Electrocatalysts for the Hydrogen Evolution Reaction in Neutral Media. *Angew. Chem., Int. Ed.* **2017**, *56*, 8120.
(41) Lu, X.; Yu, M.; Wang, G.; Tong, Y.; Li, Y. Flexible Solid-State Supercapacitors: Design, Fabrication and Applications. *Energy Environ. Sci.* **2014**, *7*, 2160.
(42) Sakthivel, M.; Ramaraj, S.; Chen, S.-M.; Chen, T.-W.; Ho, K.-C. Transition-Metal-Doped Molybdenum Diselenides with Defects and Abundant Active Sites for Efficient Performances of Enzymatic Biofuel Cell and Supercapacitor Applications. *ACS Appl. Mater. Interfaces* **2019**, *11*, 18483.
(43) Chi, K.; Zhang, Z.; Xi, J.; Huang, Y.; Xiao, F.; Wang, S.; Liu, Y. Freestanding Graphene Paper Supported Three-Dimensional Porous Graphene-Polyaniline Nanocomposite Synthesized by Inkjet Printing and in Flexible All-Solid-State Supercapacitor. *ACS Appl. Mater. Interfaces* **2014**, *6*, 16312.
(44) Chen, W.; Rakhi, R. B.; Alshareef, H. N. Facile Synthesis of Polyaniline Nanotubes using Reactive Oxide Templates for High Energy Density Pseudocapacitors. *J. Mater. Chem. A* **2013**, *1*, 3315.
(45) Yang, X.; Zhang, F.; Zhang, L.; Zhang, T.; Huang, Y.; Chen, Y. A High-Performance Graphene Oxide-Doped Ion Gel as Gel Polymer Electrolyte for All-Solid-State Supercapacitor Applications. *Adv. Funct. Mater.* **2013**, *23*, 3353.
(46) Weng, Z.; Su, Y.; Wang, D.-W.; Li, F.; Du, J.; Cheng, H.-M. Graphene-Cellulose Paper Flexible Supercapacitors. *Adv. Energy Mater.* **2011**, *1*, 917.
(47) Choudhary, N.; Li, C.; Moore, J.; Nagaiah, N.; Zhai, L.; Jung, Y.; Thomas, J. Asymmetric Supercapacitor Electrodes and Devices. *Adv. Mater.* **2017**, *29*, 1605336.
(48) Bora, A.; Mohan, K.; Doley, S.; Dolui, S. K. Flexible Asymmetric Supercapacitor Based on Functionalized Reduced Graphene Oxide Aerogels with Wide Working Potential Window. *ACS Appl. Mater. Interfaces* **2018**, *10*, 7996.
(49) Portet, C.; Yushin, G.; Gogotsi, Y. Electrochemical Performance of Carbon Onions, Nanodiamonds, Carbon Black and Multiwalled Nanotubes in Electrical Double Layer Capacitors. *Carbon* **2007**, *45*, 2511.
(50) Nagasubramanian, G.; Jungst, R. G.; Doughty, D. H. Impedance, Power, Energy, and Pulse Performance Characteristics of Small Commercial Li-Ion Cells. *J. Power Sources* **1999**, *83*, 193.

https://dx.doi.org/10.1021/acsami.9b23123
ACS Appl. Mater. Interfaces 2020, 12, 16342−16349